Article

Discovery Medicine 2025; 37(195): 750–764
https://doi.org/10.24976/Discov.Med.202537195.65

SPAG4 Regulates Glycolytic Metabolism in HT29 Cells as a Target via the c-MYC/SULT2B1 Pathway

Honghong He[1,†], Xuebing Zhang[2,*,†], Liting Zhong[2], Ting Li[2], Jinquan Ding[1], Shilai Wen[2]

[1]Radiotherapy Department, Ganzhou Cancer Hospital, 341000 Ganzhou, Jiangxi, China
[2]Oncology Department, Ganzhou People's Hospital, 341000 Ganzhou, Jiangxi, China
*Correspondence: zhangxuebing886@163.com (Xuebing Zhang)
[†]These authors contributed equally.
Published: 20 April 2025

Background: Glycolytic metabolism has been identified as a facilitator of tumor cell proliferation. Therefore, this study aims to investigate the mechanisms by which the sperm-associated antigen 4 (SPAG4)/cellular myelocytomatosis oncogene (c-Myc)/sulfotransferase 2B1 (SULT2B1) axis regulates glycolytic metabolism and influences the viability of HT29 cells.
Methods: SPAG4, c-Myc, and SULT2B1 levels were assessed in HT29 cells using Quantitative Real-Time Polymerase Chain Reaction (qRT-PCR) and Western blot analyses. Moreover, overexpression and knockdown in HT29 cell models were successfully established. Furthermore, cell viability and proliferation were evaluated using Cell Counting Kit-8 (CCK-8) and colony formation assays. Various key parameters such as glucose uptake, lactate production, Adenosine Triphosphate (ATP)/Adenosine Diphosphate (ADP) ratio, and the expression levels of Glucose transporter 1 (GLUT1) and Lactate dehydrogenase A (LDHA) were determined to examine glycolytic metabolism. Additionally, the relationship between SPAG4, c-Myc, SULT2B1, and glycolysis was assessed using the immunofluorescence staining approach and 2-Deoxy-D-glucose (2-DG) therapy.
Results: The expression levels of SPAG4, c-Myc, and SULT2B1 were significantly elevated in HT29 cells ($p < 0.05$). Moreover, silencing SPAG4 and c-Myc substantially reduced glycolytic metabolism and suppressed HT29 cell viability and colony formation capability ($p < 0.05$). Additionally, elevated SULT2B1 expression effectively counteracted the glycolytic reduction induced by silencing SPAG4 and c-Myc, enhancing cellular viability and colony formation capability ($p < 0.05$).
Conclusions: In summary, SPAG4 knockdown effectively suppresses HT29 cell proliferation and colony formation ability by decreasing SULT2B1 expression through the downregulation of c-Myc, leading to the reduction of glycolytic metabolism.

Keywords: colon cancer; glycolysis; sperm-associated antigen 4; cellular myelocytomatosis oncogene; sulfotransferase 2B1; proliferation

Introduction

Colon cancer (CC) is a malignant tumor with a significantly high global mortality rate, with its pathogenesis intricately intertwined within complex cellular signaling pathways and molecular regulatory networks [1,2]. Recently, research has increasingly investigated sperm-associated antigen 4 (SPAG4) [3]. Initially known for its crucial role in the reproductive system, emerging evidence underscores its substantial contribution to the onset and progression of various cancers [4,5]. However, a comprehensive understanding of the precise function of SPAG4 and its molecular mechanisms in CC remain unexplored, necessitating further thorough investigation.

Glycolysis, a fundamental metabolic pathway crucial for sustaining the survival and proliferation of cancer cells, plays a pivotal role in CC development [6,7]. Previous studies have reported a strong correlation between the downregulation of SPAG4 and a substantial reduction in glycolytic metabolism in CC cells [5,8]. The cellular myelocytomatosis oncogene (c-Myc), a key transcription factor, is strongly linked to the overactivation driving the onset and progression of various cancers [9,10]. Moreover, research suggests that downstream effectors of c-Myc, particularly Sulfotransferase 2B1 (SULT2B1), may modulate key steps of glycolysis, thereby impeding the proliferation of CC cells [11].

This comprehensive exploration of SPAG4 in CC enhances our understanding of its novel functions in cancer biology, unveiling valuable insights for identifying therapeutic targets. By assessing the correlation between SPAG4 and the c-Myc/SULT2B1 signaling pathway, we envisage laying a theoretical foundation for developing more precise and personalized treatment strategies. Furthermore, a comprehensive understanding of SPAG4's role in the metabolic regulation of CC may open new avenues for anticancer drug research. Through this study, we aim to advance knowledge in cancer metabolism regulation, ultimately providing more effective treatment options for patients.

Table 1. Transfection sequences used in this study.

	Sense (5′-3′)	Antisense (5′-3′)
Sh-NC	GCGCGCTTTGTAGGATTCGCAAGCTGACT GACCTTTCAAGAGAAGGTCAGTCAGCTTG CGAATCCTACAAAGCGCGC	GCGCGCTTTGTAGGATTCGCAAGCTGACT GACCTTCTCTTGAAAGGTCAGTCAGCTTG CGAATCCTACAAAGCGCGC
Sh-*SPAG4*	GATCCGCATCTTCCAGGAAGAGTACTCGA GTACTCTTCCTGGAAGATGCTTTTTTG	AATTCAAAAAAGCATCTTCCAGGAAGAGT ACTCGAGTACTCTTCCTGGAAGATGCG
Sh-*c-Myc*	GATCCGAGTCTAGTTGAGGAGGAAGTGA GGAGGAGGAAGAGCTCATAGTGGCCTGC TGAAAGCTTCA	AGCTTGAGCTTTCAGCAGGCCACTATGAG CTCTTCCTCCTCCTCACTTCCTCCTCCTCA ACTAGACTC
Ov-NC	GATCTCGAGCGGCCGCTCGAG	AATCTCGAGCGGCCGCTCGAG
Ov-*SPAG4*	CCAAGCTTGCCACCAGGATGCGGCGAAGC TCCCG	GCCTCGAGATGGGGCCCCTGTGCACTGC
Ov-*c-MYC*	GATCTCGAGCCACCATGGAACAAAAACTC ATCTCAGAAGAGGATCTG	AATCTCGAGAGATCCTCTTCTGAGATGAG TTTTTGTTCCATGGTGGCTCGAG
Ov-*SULT2B1*	GATCCCGGGCCACCATGGAGGAGGCTGCT GCT	AATTCAGCAGCAGCCTCCTCCATGGTGGC CCGGG

SPAG4, Sperm-associated antigen 4; *c-Myc*, cellular myelocytomatosis oncogene; *SULT2B1*, sulfotransferase 2B1.

Table 2. Primer sequences used in qRT-PCR.

Prime name	Prime sequence (5′-3′)
SPAG4-F	CCGCCACCAGGATGCGGCGAAGCTCCCG
SPAG4-R	GGAAATGGGGCCCCTGTGCACTG
c-Myc-F	CTGAGACAGATCAGCAACAACC
c-Myc-R	TTGTGTGTTCGCCTCTTGAC
Ki67-F	TATCAAAAGGAGCGGGGTCG
Ki67-R	ACCCCTTCCAAACAAGCAGG
LDHA-F	CGTCAGCAAGAGGGAGAAAG
LDHA-R	GCCACGTAGGTCAAGATATCC
GLUT1-F	CGGGCCAAGAGTGTGCTAAA
GLUT1-R	TGACGATACCGGAGCCAATG
β-actin-F	TCATGAAGTGTGACGTTGACATCCGTAAAG
β-actin-R	CGTAGAAGCATTTGCGGTGCACGATGGAGG

qRT-PCR, Quantitative Real-Time Polymerase Chain Reaction; *Ki67*, Marker of Proliferation Ki-67; *LDHA*, Lactate dehydrogenase A; *GLUT1*, Glucose transporter 1; F, Forward; R, Reverse.

Materials and Methods

Cell Culture

The human CC cells (HT29, iCell-h078) and colon epithelial cells (NCM460, iCell-h373) were sourced from the iCell Bioscience Inc (Shanghai, China) and cultured in a CO_2 incubator at 37 °C. These cells were cultured in their specific medium (such as HT29 in iCell-h078-001b, iCell Bioscience Inc, Shanghai, China, and NCM460 in iCell-h373-001b, iCell Bioscience Inc, Shanghai, China). Lentiviral constructs (pLVX) for SPAG4 and c-Myc (both overexpression and knockdown), SULT2B1 (overexpression), and a control vector were acquired from Sangon Biotech Co., Ltd. (Shanghai, China). Transfection sequences are shown in Table 1. Cells were transfected following the lentiviral transfection protocol provided by the manufacturer using an appropriate lentivirus quantity at a multiplicity of infection (MOI) of 5. After forty-eight hours of incubation, puromycin (60210ES25, Yasen Company, Shanghai, China) was introduced to establish stable cell lines. A Quantitative Real-Time Polymerase Chain Reaction (qRT-PCR) was conducted to validate *SPAG4*, *c-Myc*, and *SULT2B1* expression levels, ensuring the efficiency of the established cell lines. All cell lines employed in this study were authenticated using Short Tandem Repeat (STR) analysis and tested for mycoplasma contamination.

Quantitative Real-Time Polymerase Chain Reaction (qRT-PCR) Analysis

Total RNA was isolated using the TRNzol Universal reagent (DP424, TIANGEN BIOTECH CO., Ltd., Beijing, China). Genomic DNA elimination and complementary DNA synthesis were achieved using the FastQuant cDNA first strand synthesis kit (KR116) and SuperReal flu-

orescence quantitative premix reagent (FP205, TIANGEN BIOTECH CO., Ltd., Beijing, China). mRNA expression levels were determined using the PikoRealTM Real-Time PCR system (LightCycler96, Roche, Basel, Switzerland). Moreover, relative quantification was conducted employing the $2^{-\Delta\Delta Ct}$ method, with all data normalized to the internal reference β-Actin. Specific primer sequences utilized in this study are shown in Table 2.

Western Blot Analysis

Protein quantification was performed utilizing the BCA assay kit (E112-01, Vazyme, Nanjing, China). For electrophoresis, 30 µg of total protein was loaded onto a 10% polyacrylamide gel and run at 80–120 V for 90 min. The proteins were then transferred onto a Polyvinylidene fluoride (PVDF) membrane at a constant voltage of 100 mV. The membrane was immersed in a 5% bovine serum albumin solution at 25 °C for 1 hour followed by overnight incubation at 4 °C with primary antibodies against SPAG4 (1:1000; 19721-1-AP), c-Myc (1:1000; 10828-1-AP), SULT2B1 (1:1000; 29185-1-AP), and β-tubulin (1:1000; 80713-1-RR). All primary antibodies were purchased from Proteintech (Wuhan, China). The next day, the membrane was rinsed and incubated with secondary antibodies (1:2000; ZB-2305, ZB-2301; ZSGB-BIO, Beijing, China) at 25 °C for 1 hour. Finally, proteins were detected using a chemiluminescence enhancement kit (P0018AS) from Beyotime (Shanghai, China), with GAPDH serving as the internal reference. ImageJ software (version 1.5f, National Institutes of Health, Bethesda, MD, USA) was employed to analyze the grayscale values of the target bands.

Cell Counting Kit-8 (CCK-8) Assay

Following the transfection with lentiviruses, the 3×10^3 HT29 cells were cultured in 96-well plates (Servicebio, Wuhan, China) and incubated at 37 °C in the presence of 5% CO_2. CCK-8 solution (MA0218, Dalian Meilun Biotechnology Co., Ltd., Dalian, China) was applied at intervals of 72 hours, followed by incubation in the dark for 2 hours. Finally, absorbance was examined at 450 nanometers (nm), employing a microplate reader (Cmax plus, Molecular Devices, Silicon Valley, CA, USA). Cell viability was determined using the following formula:

$$\text{Cell viability } (\%) = (A1 - A0)/(A2 - A0) \times 100$$

A0: Blank hole absorbance; A1: Absorbance of transfected cells; A2: No transfected cell absorbance.

Clone Formation Assay

A total of 1×10^3 HT29 cells in the logarithmic growth phase underwent trypsinization using 0.25% trypsin to create a homogeneous single-cell suspension. Following cell counting, 1000 cells were carefully seeded into each well of a 12-well plate and uniformly distributed through gentle agitation. Subsequently, the cells were incubated at 37 °C with 5% CO_2, with regular medium replenishment every 2 days. The experiment was concluded once more than 50 distinct cell colonies were observed under the microscope, typically within 7 to 14 days.

After colony formation, the cells were meticulously fixed with 4% paraformaldehyde for 15 minutes and stained with 1% crystal violet for 10 minutes. After discarding the crystal violet staining solution, the wells were gently washed with running water, and the cells were air-dried. Finally, the colonies were photographed using an Olympus CX53 microscope (Tokyo, Japan), and the number of colonies per well was then accurately documented.

Glucose Uptake Assay

Lentivirus-transfected HT29 cells were seeded to a 6-well plate at a density of 1×10^5 cells/well containing a serum-free medium. After 24 hours of incubation, culture media was centrifuged to obtain the supernatant. Glucose uptake was determined using a glucose assay kit (BC2505, Solaibao Technology Co. Ltd., Beijing, China), and the absorbance level of each sample was measured at 505 nm employing a spectrophotometer (Cmax plus, Molecular Devices Corporation, Silicon Valley, CA, USA). Total glucose uptake was calculated as follows:

$$\text{Glucose Uptake } = (C \times V1) \times (A1 - A) \div (A2 - A) \div (5 \times V1 \div V2)$$

C: Glucose standard tube concentration (2 µmol/mL); A: Blank hole absorbance; A1: Sample hole absorbance; A2: Glucose standard absorbance; V1: Sample volume; V2: Total sample volume.

Lactic Acid Production Assay

Following the protocol of the lactic acid determination kit (BC2235, Solaibao Technology Co. Ltd., Beijing, China), a standard curve was generated using lactate standards (20 µmol/mL). HT29 cells were seeded in a 96-well plate at a density of 5000 cells per well. A 20 µL of supernatant, 26 µL of buffer, and 2 µL of lactate enzyme were thoroughly mixed, followed by incubation at room temperature for 30 minutes. Subsequently, the absorbance at 570 nm was ascertained using a microplate reader (Cmax plus, Molecular Devices Corporation, Silicon Valley, CA, USA). Lactic acid levels in the supernatant were determined utilizing a standard curve, enabling an accurate evaluation of lactic acid production by the cells. This method precisely determines the lactic acid concentration based on the established standard curve, providing valuable insights into cellular metabolic activity.

Adenosine Triphosphate (ATP)/Adenosine Diphosphate (ADP) Assay

Transfected HT29 cells into a 6-well plate at a density of 1×10^5 cells/well. After incubation in a serum-free medium for 24 hours, the media was centrifuged to collect the supernatant. The Adenosine Triphosphate (ATP)/Adenosine Diphosphate (ADP) ratio was assessed using the corresponding assay kit (MAK135-1KT, Merck, Darmstadt, Germany), following the manufacturer's instructions. Finally, chemiluminescence was observed using Microplate Readers (Cmax plus, Molecular Devices Corporation, Silicon Valley, CA, USA).

TUNEL Assay

HT29 cell apoptosis was assessed using the TUNEL kit (T2130, Solarbio, Beijing, China). After culture in 12-well plates, the 5×10^7 cells were washed twice with phosphate-buffered saline (PBS) (C1088, Beyotime Biotechnology, Shanghai, China) and then fixed in 4% paraformaldehyde for 25 minutes. After soaking in Triton X-100 for 10 min, the cells underwent staining with 50 µL Terminal deoxynucleotidyl transferase (TdT) solution and 450 µL fluorescein-labeled Deoxyuridine triphosphate (dUTP) solution for 60 min in the dark. The cells were then stained with 4′, 6-diamino-2-phenylindole (DAPI) for 15 min, and the positive cells were observed under a fluorescence microscope (LY19, Olympus, Tokyo, Japan).

EdU Assay

The proliferation of HT29 cells (1×10^4 cells/well, 1 mL/well) after different treatments was determined using the 5-Ethynyl-2′-deoxy uridine (EdU) kit (C10310, RIBOBIO, Guangzhou, China). The growth phase cells were isolated and inoculated into 96-well plates at a density of 1×10^5 cells per well. Then, 100 µL 50 µM EdU medium was added to each well and incubated for 2 h. The EdU medium was then discarded, and the cells underwent two washes with PBS. Each well was added with 50 µL cell fixative (PBS containing 4% paraformaldehyde) and incubated at room temperature for 30 min. After this, 100 µL penetrant (PBS of 0.5% TritonX-100) was added, followed by a 10-minute incubation in a shaker. The cells were then stained with DAPI (D1306, Invitrogen, Carlsbad, CA, USA), and the positive HT29 cells were examined under a fluorescence microscope (LY19, Olympus, Tokyo, Japan).

Immunofluorescence Staining

HT29 cells were immobilized on a slide with 4% paraformaldehyde, impregnated with 0.5% Triton X-100 for 20 minutes, and blocked with 2% goat serum for 1 hour. The cells then underwent an overnight incubation at 4°C with the primary antibodies against c-Myc (1:1000, 700648), SPAG4 (1:1000, PA5-49730), and SULT2B1 (1:1000, MA5-55948).

The following day, the cells were incubated with the secondary antibodies (1:2000, A32723, or A-31573) at room temperature for one hour in the dark. All antibodies were obtained from Thermo Fisher Scientific (Waltham, MA, USA). The cells were treated with 5mM 2-DG for 24h. [12]. The cells were observed under a fluorescence microscope (LY19, Olympus, Tokyo, Japan) to record the images, and the fluorescence intensity was analyzed using ImageJ (version 1.5f, National Institutes of Health, Bethesda, MD, USA).

Statistical Analyses

Statistical analyses were performed utilizing GraphPad Prime software 8.0 (GraphPad Prime Inc, San Diego, CA, USA, accessible at https://www.graphpad-prism.cn/). The results were expressed as mean ± standard deviation. *T*-tests and Analysis of Variance (ANOVA) with Tukey's post hoc analysis were used to statistically examine significant differences and trends. Statistical significance was established at a p-value of <0.05.

Results

Downregulation of SPAG4 Inhibited the Proliferation of HT29 Cells

To comprehensively evaluate the expression profiles of SPAG4 and c-Myc in HT29, their expression in HT29 and normal colonic epithelial cells was analyzed using qRT-PCR and Western blot analyses. As shown in Fig. 1A–E, SPAG4 and c-Myc were substantially upregulated in HT29 cells compared to normal colonic epithelial cells ($p < 0.05$).

To delve deeper into the interaction between SPAG4 and c-Myc in HT29 cells, a stable SPAG4 knockdown model was established. This analysis allowed us to assess the regulatory influence of SPAG4 on c-Myc expression and its functional attributes in HT29 cells. As depicted in Fig. 1F–H, SPAG4 knockdown significantly reduced c-Myc protein levels ($p < 0.05$). Furthermore, SPAG4 knockdown substantially decreased the expression of Ki67 ($p < 0.05$, Fig. 1I). Additionally, the inhibition of SPAG4 significantly suppressed the proliferation and colony-forming capability of HT29 cells ($p < 0.05$, Fig. 1J–L).

Knocking Down SPAG4 Suppressed the Proliferation of HT29 Cells by Downregulating c-Myc

To further substantiate the role of SPAG4 in promoting proliferation within HT29 cells through the regulation of c-MYC, both SPAG4 knockdown and c-Myc overexpression strategies were implemented. As shown in Fig. 2A–C, a significant reduction was observed in SPAG4 and c-Myc protein expression levels following SPAG4 knockdown in HT29 cells ($p < 0.05$, **Supplementary Fig. 1A,B**). However, after administering Sh-SPAG4, the introduction of Ov-c-Myc significantly increased the c-Myc protein level in HT29 cells ($p < 0.05$), while changes in SPAG4 lev-

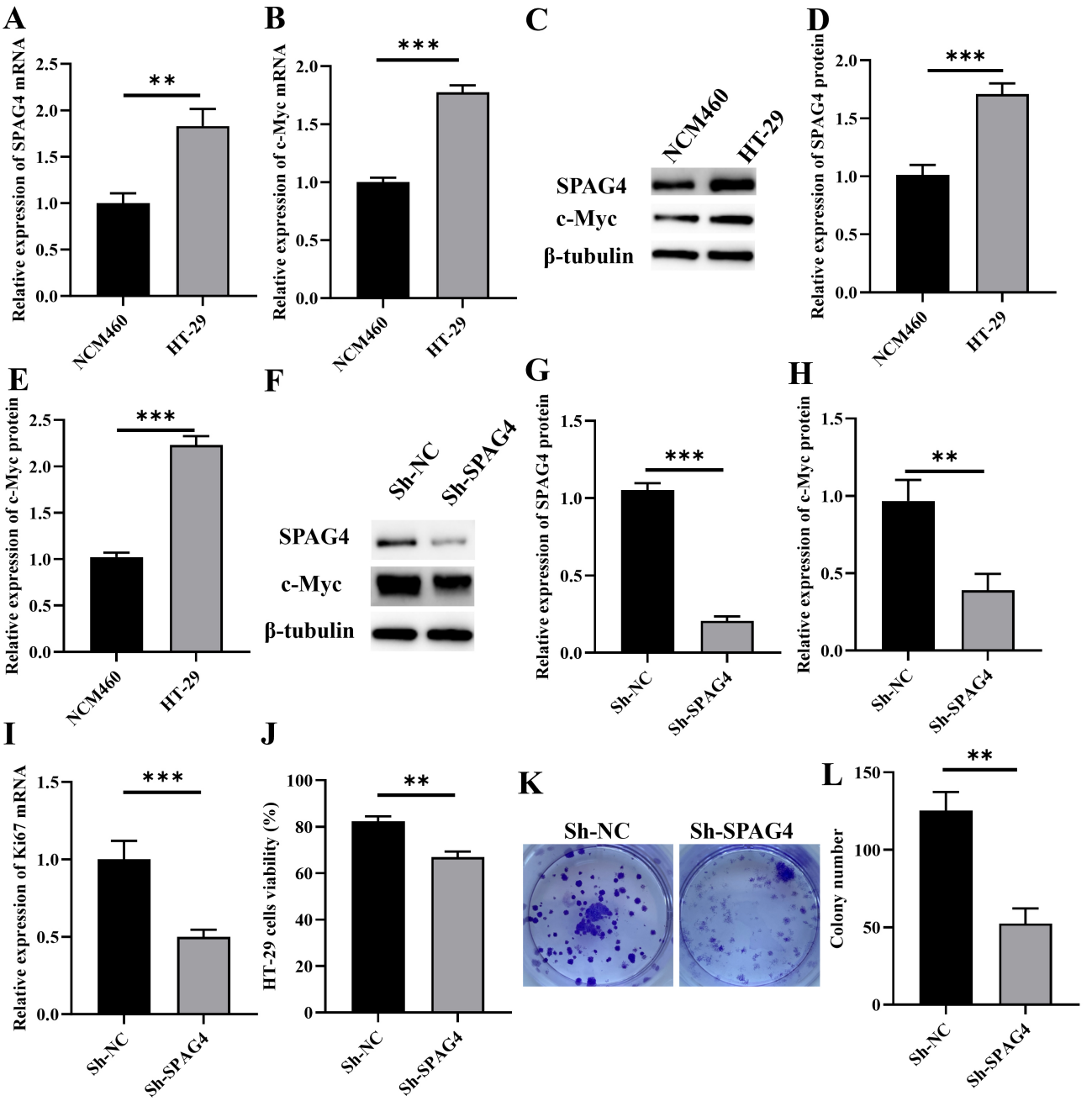

Fig. 1. The SPAG4 knockdown inhibited the expression of c-Myc and the proliferation of HT29 cells. (A,B) mRNA expression levels of *SPAG4* (A) and *c-Myc* (B) in HT29 cells and NCM460 cells were assessed using qRT-PCR. (C–E) Western blot analysis was used to examine the protein expression levels of SPAG4 and c-MYC in both HT29 cells and NCM460 cells. (F–H) After *SPAG4* gene knockout, the changes in SPAG4 and c-Myc protein expression levels across HT29 cells were determined using Western blot analysis. (I) qRT-PCR was utilized to measure the mRNA levels of *Ki67* to determine proliferative activity. (J) A Cell Counting Kit-8 (CCK-8) assay was executed to examine the viability of HT29 cells. (K,L) A colony formation assay was performed to evaluate the colony-forming ability of HT29 cells (n = 3) (**$p < 0.01$, ***$p < 0.001$). SPAG4, Sperm-associated antigen 4; c-Myc, cellular myelocytomatosis oncogene; Ki67, Marker of Proliferation Ki-67.

els remained insignificant ($p > 0.05$). Additionally, CCK-8 assay, colony-forming experiment, and qRT-PCR analysis demonstrated a substantial enhancement in cellular viability ($p < 0.05$), colony formation ($p < 0.05$), and Ki67 expression ($p < 0.05$) in HT29 cells following Sh-SPAG4+Ov-Myc treatment (Fig. 2D–G). Intriguingly, this effect was counteracted by Ov-c-Myc treatment ($p < 0.05$), highlighting a strong interaction between SPAG4 and c-Myc in regulating key cellular processes during CC.

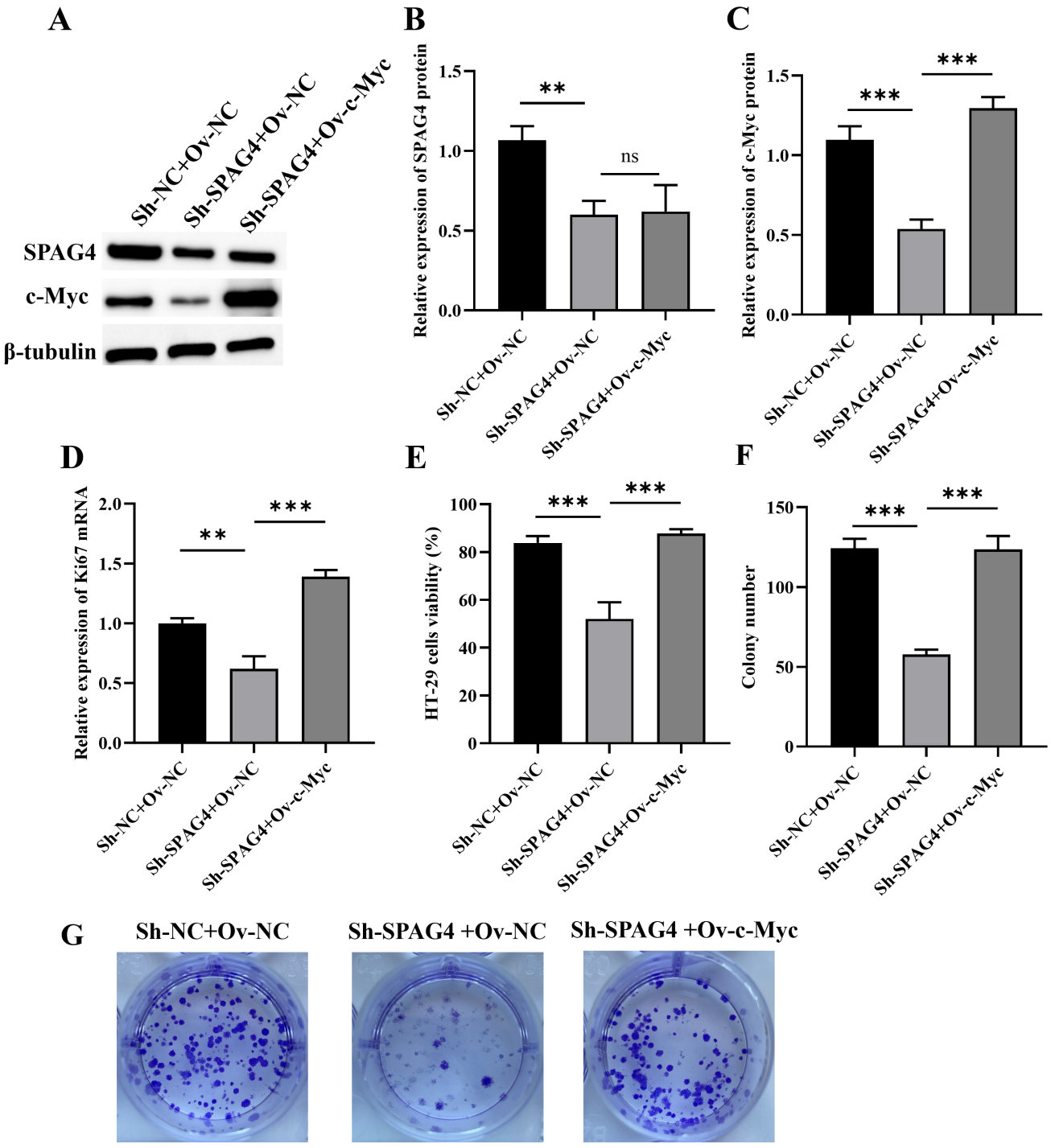

Fig. 2. SPAG4 knockdown downregulated c-Myc and inhibited the proliferation of HT29 cells. (A–C) Western blot analysis was used to examine the expression levels of SPAG4 and c-Myc proteins in HT29 cells. (D) qRT-PCR was employed to evaluate the mRNA expression of *Ki67* in HT29 cells. (E) CCK-8 assay was implemented to determine the viability of HT29 cells. (F,G) The colony formation assay was conducted to evaluate the colony-forming ability of HT29 cells (n = 3) (ns, no significant difference, $^{**}p < 0.01$, $^{***}p < 0.001$).

Knocking Down c-Myc Decreased SULT2B1 Expression and Inhibited the Glycolytic Metabolism of HT29 Cells

Western blot analysis revealed a significant upregulation of SULT2B1 expression in HT29 cells compared to colonic epithelial cells ($p < 0.05$, Fig. 3A,B). Moreover, lentivirus-mediated suppression of c-Myc in HT29 cells led to a substantial reduction in c-Myc and SULT2B1 expression levels ($p < 0.05$, Fig. 3C–E). Further exploration into glycolytic metabolism indicators showed that c-

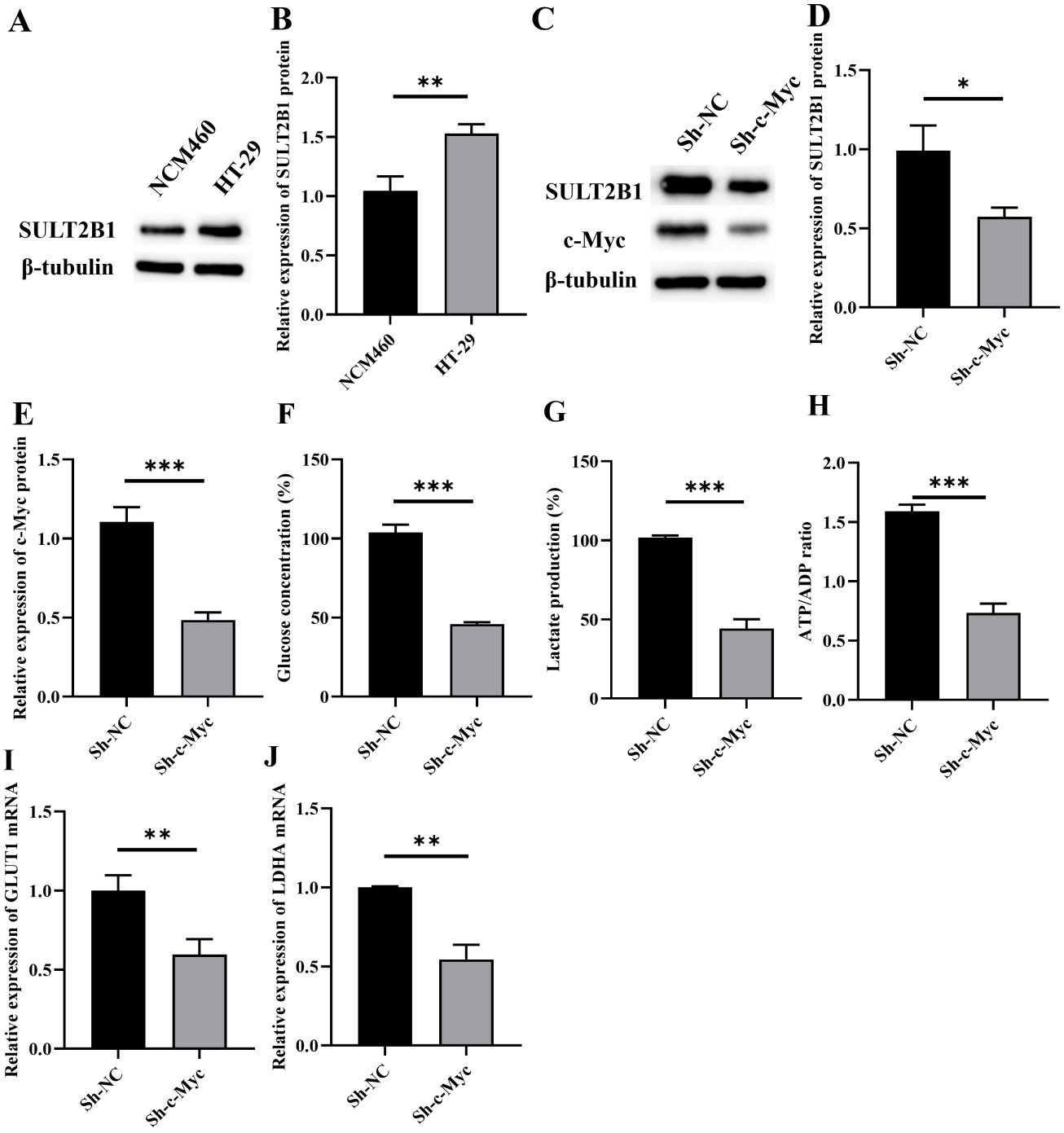

Fig. 3. c-Myc knockdown decreased SULT2B1 expression and inhibited the glycolytic metabolism of HT29 cells. (A,B) SULT2B1 protein expression in HT29 cells and normal colonic epithelial cells was assessed using Western blot analysis. (C–E) Protein expression of c-Myc and SULT2B1 in HT29 cells was determined using Western blot analysis. (F) Measurement of glucose levels in HT29 cells. (G) An evaluation of lactate production in HT29 cells. (H) The Adenosine Triphosphate (ATP)/Adenosine Diphosphate (ADP) ratio in HT29 cells. (I,J) qRT-PCR was employed to measure the mRNA expression of *GLUT1* and *LDHA* in HT29 cells (n = 3) (*$p < 0.05$, **$p < 0.01$, ***$p < 0.001$).

Myc knockout substantially decreased glucose uptake ($p < 0.05$), lactate production ($p < 0.05$), ATP/ADP ratio ($p < 0.05$), and the expression levels of GLUT1 and LDHA ($p < 0.05$) in HT29 cells (Fig. 3F–J). These findings underscore the pivotal regulatory role of c-Myc in modulating glycolytic metabolism in HT29 cells. In summary, the increased expression of SULT2B1 in HT29 cells is closely linked with its downregulation of SULT2B1 and the inhibition of glycolytic metabolism after c-Myc knockdown. These observations provide valuable insights into the intri-

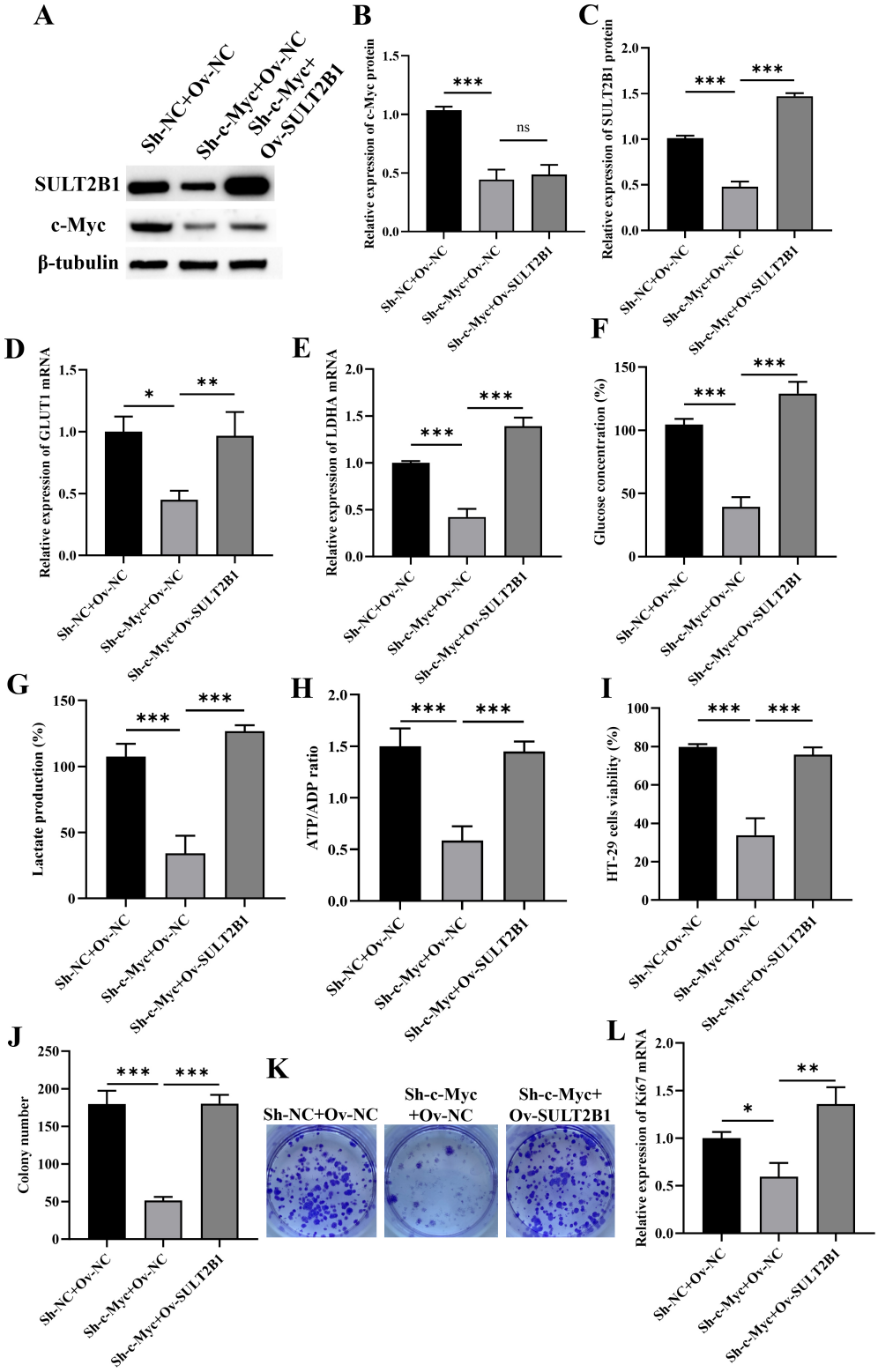

Fig. 4. The inactivation of the c-Myc/SULT2B1 axis disrupted glycolytic metabolism, thereby reducing the viability of HT29 cells. (A–C) The expression of c-Myc and SULT2B1 proteins in HT29 cells was analyzed using Western blot analysis. (D,E) qRT-PCR was employed to determine the mRNA expression of *GLUT1* and *LDHA* in HT29 cells. (F) The quantification of glucose content in HT29 cells. (G) The assessment of lactate production in HT29 cells. (H) The determination of the ATP/ADP ratio in HT29. (I) The CCK-8 assay was utilized to assess the viability of HT29 cells. (J,K) The colony formation assay was used to evaluate the colony-forming ability of HT29 cells. (L) qRT-PCR was conducted to assess *Ki67* mRNA expression in HT29 cells (n = 3) (ns, no significant difference, *$p <$ 0.05, **$p < 0.01$, ***$p < 0.001$).

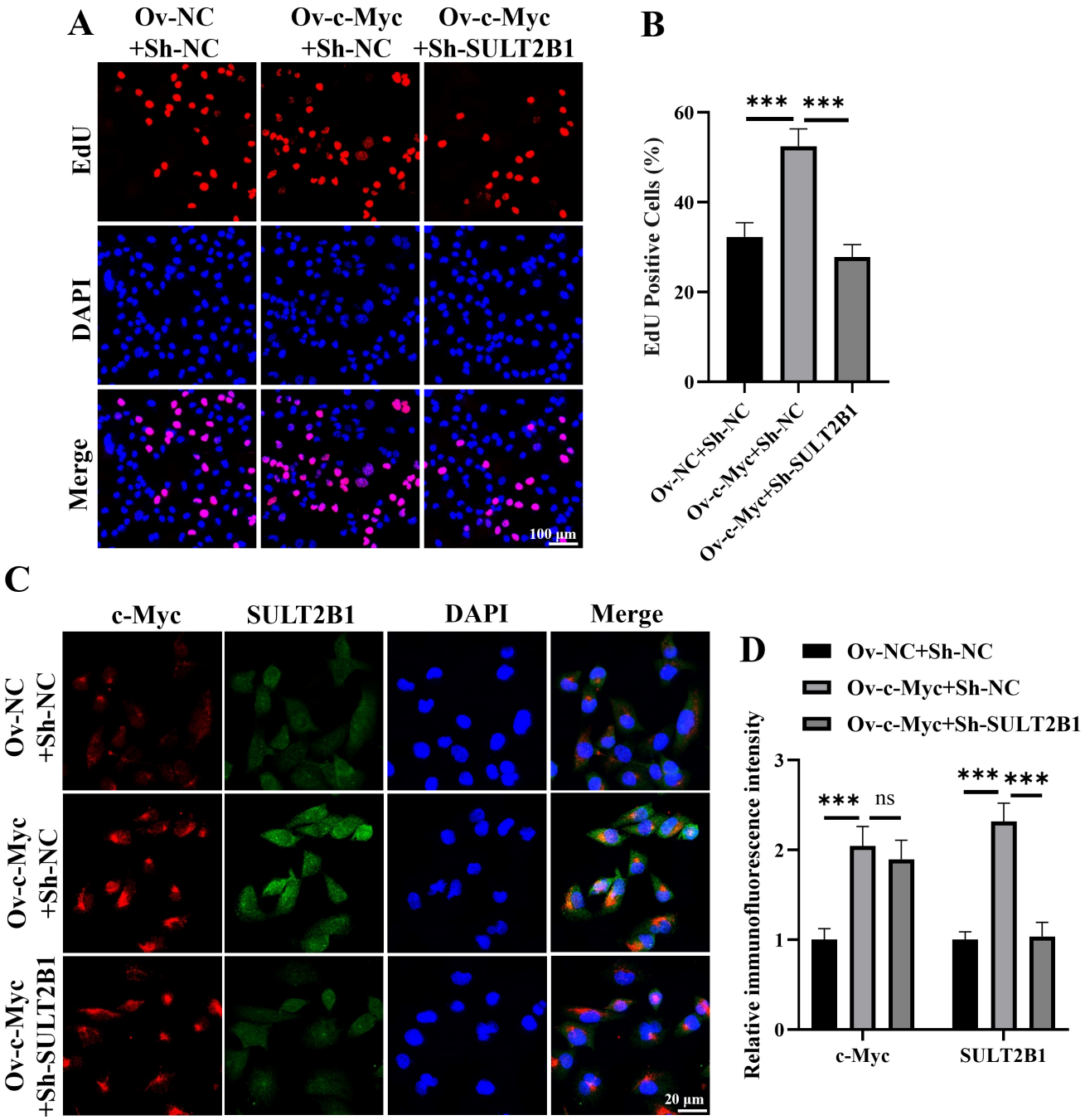

Fig. 5. Silencing SULT2B1 inhibited HT29 cell proliferation by overexpressing c-Myc. (A,B) Silencing the proliferation of HT29 cells with c-Myc and overexpression of SULT2B1. (C,D) immunofluorescence staining of c-Myc and SULT2B1 (n = 3) (ns, no significant difference, ***$p < 0.001$). DAPI, 4′, 6-diamino-2-phenylindole; EdU,5-Ethynyl-2′-deoxy uridine.

cate association between SULT2B1 and c-Myc in shaping the metabolic dynamics of HT29 cells.

Knocking Down c-Myc Suppressed HT29 Cell Proliferation by Suppressing Glycolytic Metabolism Through the Reduction of SULT2B1 Expression

To delve deeper into the regulatory role of c-Myc in glycolytic metabolism and its influence on HT29 cell proliferation through SULT2B1, we successfully established cell lines with c-Myc knockdown and SULT2B1 overexpression ($p < 0.05$, Fig. 4A–C, **Supplementary Fig. 1C,D**). We observed that SULT2B1 overexpression did not alter c-Myc expression levels after c-Myc silencing. However, crucial indicators of glycolytic metabolisms, such as glucose uptake ($p < 0.05$), lactate production ($p < 0.05$), ATP/ADP ratio ($p < 0.05$), and the expressions of glycolytic-related genes *GLUT1* ($p < 0.05$) and *LDHA* ($p < 0.05$), were significantly decreased after c-Myc silencing but were restored after SULT2B1 overexpression ($p < 0.05$, Fig. 4D–H). These results suggest that SULT2B1 overexpression re-

instates the inhibitory effect of c-Myc knockdown on glycolysis. Furthermore, the CCK-8 assay and colony formation assay collectively revealed that SULT2B1 overexpression counteracts the suppressive effects of c-Myc knockdown on HT29 cell proliferation ($p < 0.05$, Fig. 4I–K). Moreover, *Ki67* mRNA expression was significantly decreased after c-Myc silencing ($p < 0.05$) but increased after SULT2B1 overexpression ($p < 0.05$, Fig. 4L). This comprehensive analysis underscores the close link between c-Myc, SULT2B1, and glycolytic pathways, highlighting their collective role in modulating the proliferative behavior of HT29 cells.

Silencing SULT2B1 Inhibited HT29 Cell Proliferation

As shown in Fig. 5A,B, HT29 cell proliferation was enhanced after c-Myc overexpression, while HT29 cell proliferation was decreased after SULT2B1 silencing ($p < 0.05$). Furthermore, c-Myc overexpression significantly increased the fluorescence intensity of c-Myc and ($p < 0.05$, Fig. 5C,D). However, SULT2B1 silencing did not significantly affect the fluorescence intensity of c-Myc ($p > 0.05$), while it significantly reduced the fluorescence intensity of SULT2B1 ($p < 0.05$). These observations, in combination with previous results, reveal that c-Myc function upstream of SULT2B1.

Knocking Down SPAG4 Suppressed Glycolytic Metabolism by Downregulating the c-Myc/SULT2B1 Axis, Thereby Inhibiting HT29 Cell Proliferation

We successfully developed cell lines with SPAG4 knockdown and SULT2B1 overexpression ($p < 0.05$) (Fig. 6A–D). We observed that SULT2B1 overexpression did not change c-Myc or SPAG4 expression levels ($p > 0.05$). Moreover, SULT2B1 overexpression significantly increased glucose uptake, lactate production, ATP/ADP ratio, and the expression of GLUT1 and LDHA ($p < 0.05$, Fig. 6E–I). Additionally, the CCK-8 assay, colony formation assay, and Ki67 expression analysis revealed that SULT2B1 overexpression counteracts the reduction in HT29 cell viability induced by SPAG4 knockdown ($p < 0.05$, Fig. 6J–M).

SPAG4 Overexpression Promoted HT29 Cell Proliferation, Whereas SULT2B1 Silencing Inhibited Their Proliferation

As illustrated in Fig. 7A,B, SPAG4 overexpression significantly enhanced the proliferative ability of HT29 cells, whereas SULT2B1 silencing decreased their proliferation ($p < 0.05$). To further demonstrate the association of SULT2B1 and SPAG4, immunofluorescence staining was performed. As shown in Fig. 7C,D, SPAG4 overexpression significantly enhanced the immunofluorescence intensity of SPAG4 and SULT2B1, while SULT2B1 silencing significantly decreased the immunofluorescence intensity of SULT2B1 ($p < 0.05$) but did not change the immunofluorescence intensity of SPAG4 expression ($p > 0.05$). Furthermore, the glycolysis inhibitor 2-DG treatment significantly enhanced apoptosis in HT29 cells ($p < 0.05$, Fig. 7E,F). These results suggest the potential mechanistic pathway (Fig. 8), where SPAG4 promotes c-Myc expression, which upregulates SULT2B1 expression, thereby promoting glycolysis.

Discussion

This study investigates the mechanistic interplay of SPAG4/c-Myc/SULT2B1 in CC tumors, uncovering that SPAG4 depletion leads to c-MYC downregulation, consequently diminishing the transcription of SULT2B1. Consistent with the previous study, c-Myc may directly regulate SULT2B1, while SPAG4 may exert direct regulatory control over c-Myc [11]. This cascade ultimately impedes glycolytic metabolism, thereby reducing the proliferative capacity of CC cells. Further investigations reveal that SPAG4 expression is increased in CC tissues and inversely linked to patient survival outcomes. Furthermore, these findings indicate that SPAG4 overexpression actively stimulates glycolytic metabolism, supporting CC cell proliferation [5,8].

Moreover, recent research has uncovered the role of SPAG4 in tumor growth, transformation, and progression across diverse cancer cell types, highlighting its multifaceted significance in tumorigenesis and cancer cell development [13]. Previous research has indicated that SPAG4 is upregulated in renal cell carcinoma (RCC), where it's knocking down reduces the invasive capability of RCC cells *in vitro*, while overexpression increases tumor cell migration and invasion [14]. Similarly, results by Liu *et al.* [15] indicated that SPAG4 is overexpressed in hepatocellular carcinoma tissues and holds prognostic value. Wang *et al.* [16] further suggested that SPAG4 is overexpressed in lung squamous cell carcinoma compared to adjacent tissues, serving as a prognostic marker related to glycolysis.

In this context, we suggest that SPAG4 plays a vital role in the glycolytic metabolism and proliferation of HT29 cells. Given that Ki67 is widely known as a biomarker of cellular proliferation, with decreased Ki67 expression closely associated with reduced cancer cell proliferation [17], our results support the hypothesis that SPAG4 affects the metabolic and proliferative dynamics of HT29 cells. Another study has identified SPAG4 as a novel biomarker for glioblastoma, where its silencing significantly inhibits tumor cell proliferation and migration [18]. Based on these findings, we propose that SPAG4 knockout can reduce glycolytic metabolism and proliferation in HT29 cells.

Previous research has reported c-Myc as a crucial oncogenic transcription factor associated with the reprogramming, proliferation, and chemoresistance of various cancer cell types [19–21]. A recent study has indicated

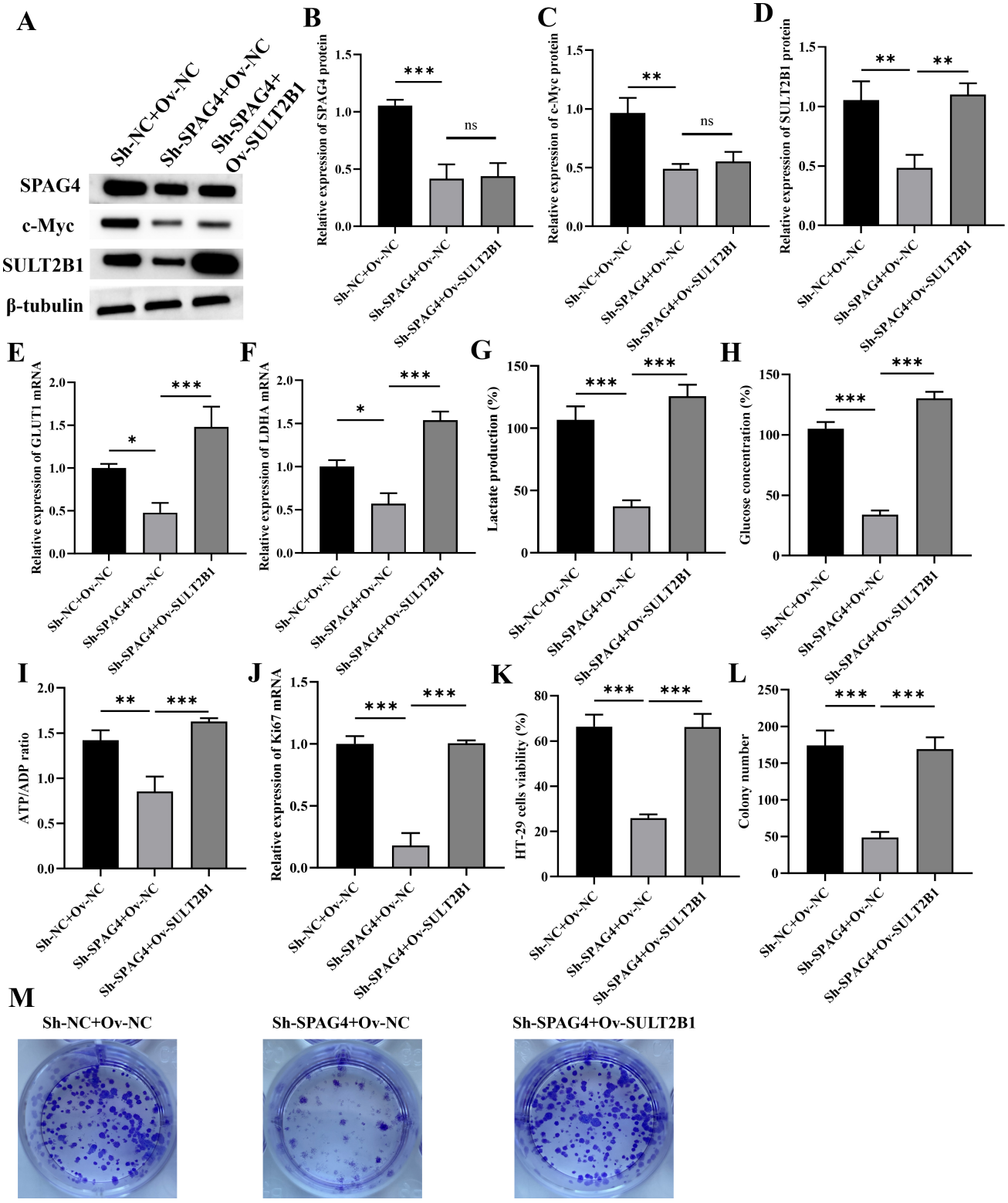

Fig. 6. Blocking the SPAG4/c-Myc/SULT2B1 axis suppressed glycolytic metabolism, thereby reducing HT29 cell viability. (A–D) Expression levels of SPAG4, c-Myc, and SULT2B1 proteins in HT29 cells were determined using Western blot analysis. (E,F) qRT-PCR was employed to measure the mRNA expression levels of *GLUT1* and *LDHA* in HT29 cells. (G) Lactate production in HT29 cells. (H) Glucose content in HT29 cells. (I) The ATP/ADP ratio in HT29 cells was determined following c-MYC knockdown. (J) qRT-PCR was used to examine mRNA *Ki67* expression levels in HT29 cells. (K) The CCK-8 assay was utilized to evaluate HT29 cell viability. (L,M) The colony formation assay was applied to assess the colony-forming ability of HT29 cells (n = 3) (ns, no significant difference, *$p <$ 0.05, **$p < 0.01$, ***$p < 0.001$).

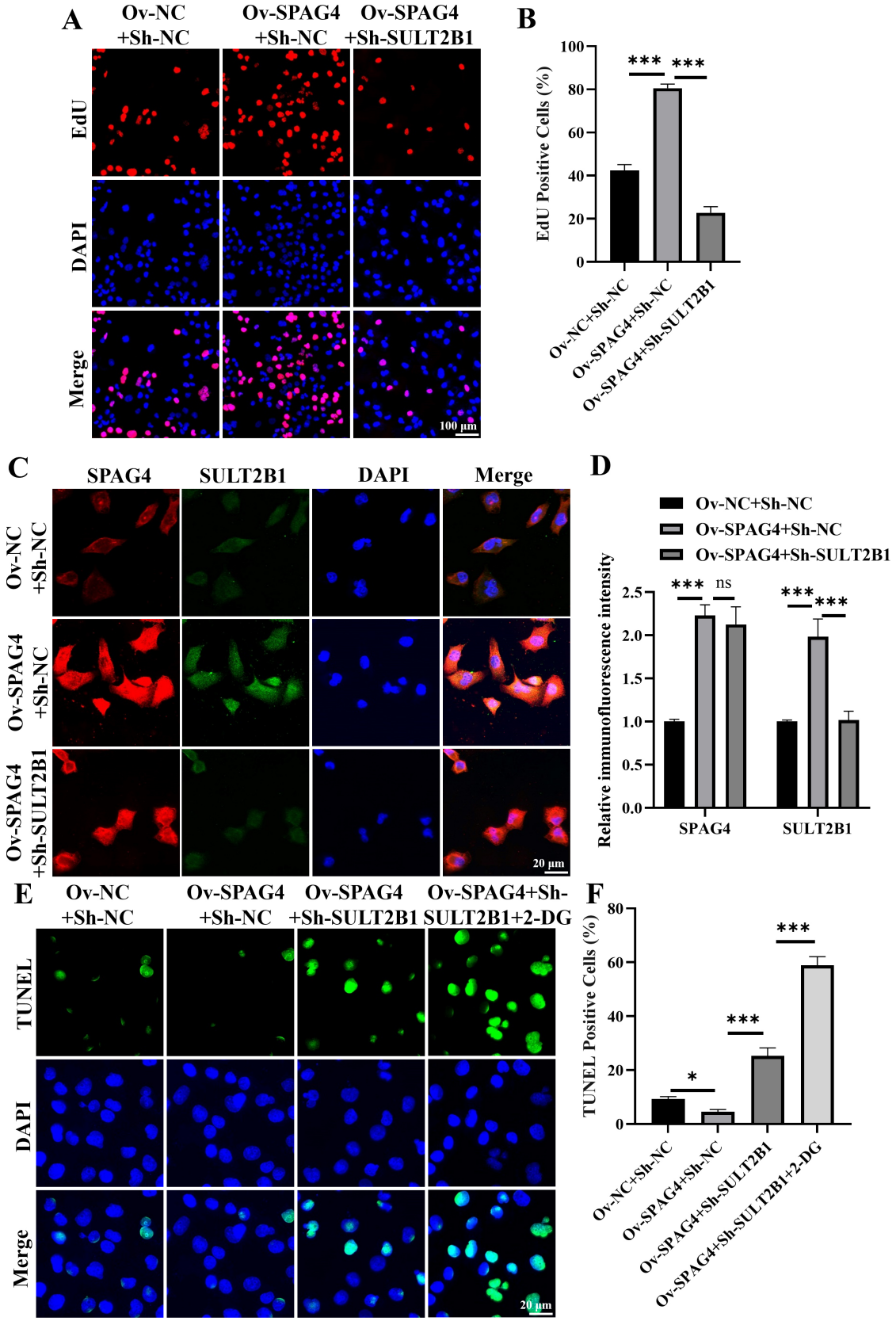

Fig. 7. SULT2B1 silencing inhibited HT29 cell proliferation by overexpressing c-Myc. (A,B) HT29 cell proliferation following SPAG4 silencing and SULT2B1 overexpression. (C,D) Immunofluorescence staining of SPAG4 and SULT2B1. (E,F) TUNEL staining determining the anti-apoptotic ability of HT29 cells after 2-Deoxy-D-glucose (2-DG) treatment (n = 3) (ns, no significant difference, * $p < 0.05$, *** $p < 0.001$).

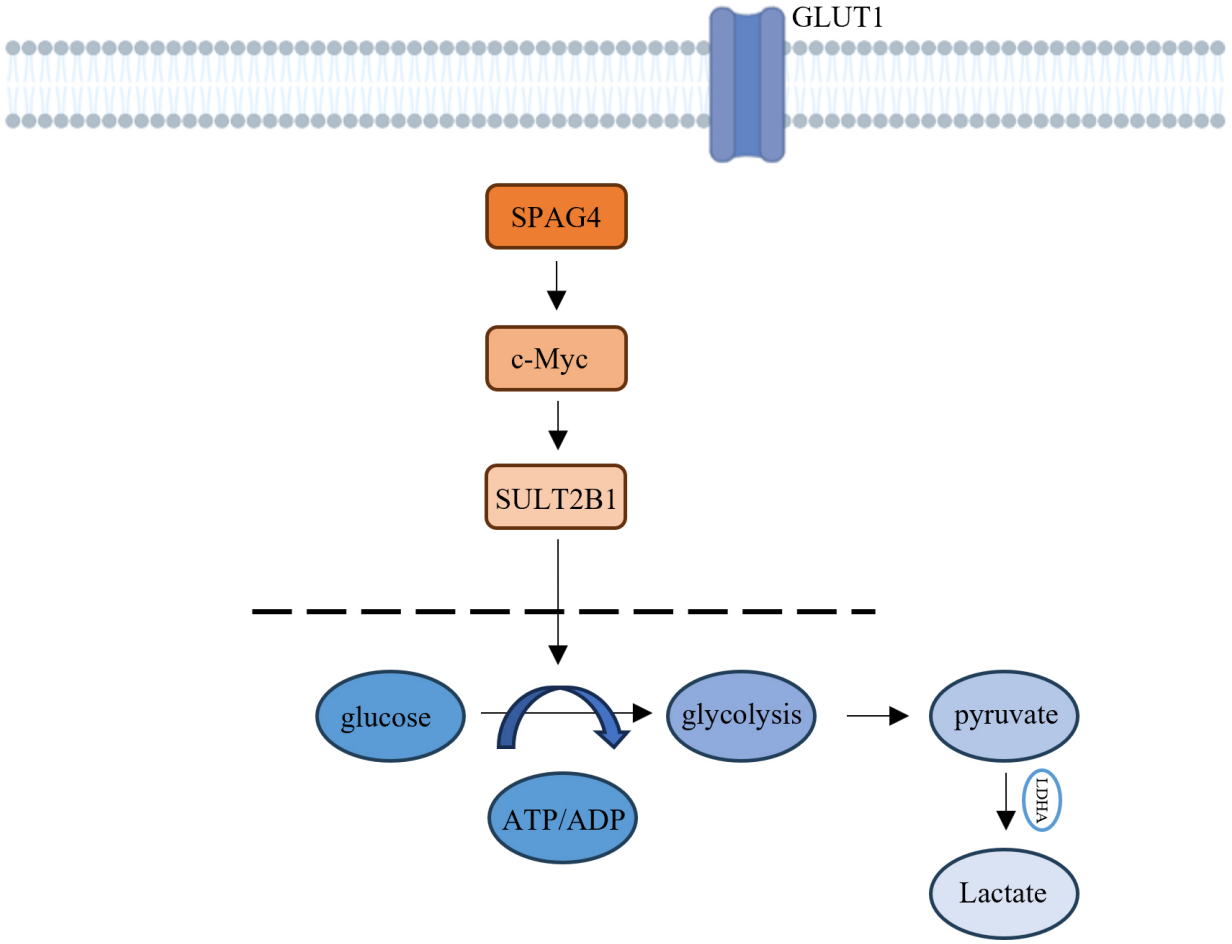

Fig. 8. SPAG4, the relationship between c-Myc and SULT2B1 and the underlying mechanism affecting HT29 cells.

that the upregulation of c-Myc significantly accelerates tumor metastasis [22]. In our study, we observed that SPAG4 knockdown reduced c-Myc expression, thereby suppressing glycolytic metabolism and proliferation of HT29 cells, a finding being observed for the first time. Lin *et al*. [23] reported that c-Myc activation significantly facilitates the viability, metastasis, and glycolysis of pancreatic cancer cells. Similarly, the downregulation of c-Myc has been shown to reduce the proliferation of HT29 and SW480 CC cells while inhibiting aerobic glycolysis, consistent with our results [24]. Moreover, the persistent expression of c-Myc is believed to be a pivotal driver of glycolytic metabolism, thereby fostering the proliferation and tumorigenic growth of colorectal cancer cells. This mechanism contributes significantly to the metabolic shifts that support the rapid division and progression of CC cells [25]. However, the precise mechanism behind c-Myc's involvement in the glycolytic metabolism of CC remains to be fully explored.

The findings from our study propose a novel perspective, indicating that c-Myc suppression leads to reduced glycolytic metabolism through the downregulation of SULT2B1, ultimately inhibiting the proliferative capacity of HT29 cells. This observation underscores the need for further investigations to unravel the detailed mechanisms underlying c-Mc/SULT2B1/glycolytic pathways in CC. Xu *et al*. [26] revealed that SULT2B1 is closely associated with the physiological function of intestinal cells, while Zhao *et al*. [11] reported that SULT2B1 knockdown disrupts CC cell viability, aligning well with our findings.

In summary, this study suggests that SPAG4 depletion disrupts the activation of the c-Myc/SULT2B1 axis, leading to glycolytic inhibition and decreased CC cell viability. This study indicates the upstream and downstream relationship between the three (SPAG4-c-Myc-SULB2T1), positions the SPAG4/c-Myc/SULB2T1 pathway as a key regulatory cascade in glycolytic metabolism and provides a potential therapeutic target in colon cancer. However, the role of SULT2B1 in glycolytic metabolism remains limited, necessitating further research to ascertain whether it plays a regulatory role in glycolysis across different cancer types. Additionally, our results show that c-Myc overexpression may increase SPAG4 expression, while SULT2B1 overexpression may increase c-Myc expression. Although these changes are statistically insignificant, they reveal a potential negative feedback phenomenon within the SPAG4/c-Myc/SULT2B1 pathway, which may have some biological

significance. Further studies are warranted to explore the significance of this regulatory mechanism and to offer more compelling evidence supporting our findings.

There are many limitations in this study. Firstly, this study exclusively relied on cell models, with a limited number of experimental samples. To further validate our results, future studies should use clinical samples and animal models. Secondly, our study focused on a single pathway, underscoring the need for further investigation to identify more targets related to this pathway. Lastly, although this study found that SPAG4 may be a critical therapeutic target, its practical application in clinical settings remains an open question. Future studies should investigate the development of tailored drugs against SPAG4 and evaluate their effectiveness through animal experiments.

Conclusions

The potential impact of SPAG4 silencing on SULT2B1 expression may be achieved through the downregulation of c-Myc. This mechanistic pathway potentially reduces glycolytic metabolism and inhibits the viability and colony formation ability of CC cells.

Availability of Data and Materials

The original contributions presented in the study are included in the article/supplementary material. Further inquiries can be directed to the corresponding author.

Author Contributions

HH: Conception, Design, Materials, Data Collection, Analysis, Literature Review, Writing. XZ: Design, Supervision, Materials, Data Collection, Analysis, Literature Review, Writing. LZ: Materials, Data Collection, Analysis, Literature Review, Writing. TL: Design, Materials, Data Collection, Analysis, Literature Review, Writing. JD: Supervision, Materials, Data Collection, Analysis, Writing. SW: Supervision, Materials, Data Collection, Analysis, Writing, Critical Review for Important Intellectual Content. All authors have read and approved the final manuscript. All authors have participated sufficiently in the work and agreed to be accountable for all aspects of the work.

Ethics Approval and Consent to Participate

Not applicable.

Acknowledgment

Not applicable.

Funding

This research received no external funding.

Conflict of Interest

The authors declare no conflict of interest.

Supplementary Material

Supplementary material associated with this article can be found, in the online version, at https://doi.org/10.24976/Discov.Med.202537195.65.

References

[1] Fabregas JC, Ramnaraign B, George TJ. Clinical Updates for Colon Cancer Care in 2022. Clinical Colorectal Cancer. 2022; 21: 198–203. https://doi.org/10.1016/j.clcc.2022.05.006.

[2] Benson AB, Venook AP, Al-Hawary MM, Arain MA, Chen YJ, Ciombor KK, *et al*. Colon Cancer, Version 2.2021, NCCN Clinical Practice Guidelines in Oncology. Journal of the National Comprehensive Cancer Network: JNCCN. 2021; 19: 329–359. https://doi.org/10.6004/jnccn.2021.0012.

[3] Liu Y, He M, Ke X, Chen Y, Zhu J, Tan Z, *et al*. Centrosome amplification-related signature correlated with immune microenvironment and treatment response predicts prognosis and improves diagnosis of hepatocellular carcinoma by integrating machine learning and single-cell analyses. Hepatology International. 2024; 18: 108–130. https://doi.org/10.1007/s12072-023-10538-5.

[4] Zhang X, Wu W, Li X, He F, Zhang L. SPAG5 promotes the proliferation, migration, invasion, and epithelial-mesenchymal transformation of colorectal cancer cells by activating the PI3K/AKT signaling pathway. The Chinese Journal of Physiology. 2023; 66: 365–371. https://doi.org/10.4103/cjop.CJOP-D-22-00165.

[5] Mao G, Wu J, Cui H, Dai L, Ma L, Zhou Z, *et al*. A Novel Glycolysis and Hypoxia Combined Gene Signature Predicts the Prognosis and Affects Immune Infiltration of Patients with Colon Cancer. International Journal of General Medicine. 2022; 15: 1413–1427. https://doi.org/10.2147/IJGM.S351831.

[6] Huang J, Yang M, Liu Z, Li X, Wang J, Fu N, *et al*. PPFIA4 Promotes Colon Cancer Cell Proliferation and Migration by Enhancing Tumor Glycolysis. Frontiers in Oncology. 2021; 11: 653200. https://doi.org/10.3389/fonc.2021.653200.

[7] Pan G, Zhang P, Chen A, Deng Y, Zhang Z, Lu H, *et al*. Aerobic glycolysis in colon cancer is repressed by naringin via the *HIF1A* pathway. Journal of Zhejiang University. Science. B. 2023; 24: 221–231. https://doi.org/10.1631/jzus.B2200221.

[8] Yi K, Wu J, Tang X, Zhang Q, Wang B, Wang F. Identification of a novel glycolysis-related gene signature for predicting the survival of patients with colon adenocarcinoma. Scandinavian Journal of Gastroenterology. 2022; 57: 214–221. https://doi.org/10.1080/00365521.2021.1989026.

[9] Loevenich LP, Tschurtschenthaler M, Rokavec M, Silva MG, Jesinghaus M, Kirchner T, *et al*. SMAD4 Loss Induces c-MYC-Mediated NLE1 Upregulation to Support Protein Biosynthesis, Colorectal Cancer Growth, and Metastasis. Cancer Research. 2022; 82: 4604–4623. https://doi.org/10.1158/0008-5472.CAN-22-1247.

[10] Zhang HL, Wang P, Lu MZ, Zhang SD, Zheng L. c-Myc maintains the self-renewal and chemoresistance properties of colon cancer stem cells. Oncology Letters. 2019; 17: 4487–4493. https://doi.org/10.3892/ol.2019.10081.

[11] Zhao T, Li Y, Shen K, Wang Q, Zhang J. Knockdown of OLR1 weakens glycolytic metabolism to repress colon cancer cell proliferation and chemoresistance by downregulating SULT2B1 via

c-MYC. Cell Death & Disease. 2021; 13: 4. https://doi.org/10.1038/s41419-021-04174-w.

[12] Bhatt AN, Kumar A, Rai Y, Kumari N, Vedagiri D, Harshan KH, *et al*. Glycolytic inhibitor 2-deoxy-d-glucose attenuates SARS-CoV-2 multiplication in host cells and weakens the infective potential of progeny virions. Life Sciences. 2022; 295: 120411. https://doi.org/10.1016/j.lfs.2022.120411.

[13] Ji Y, Jiang J, Huang L, Feng W, Zhang Z, Jin L, *et al*. Sperm associated antigen 4 (SPAG4) as a new cancer marker interacts with Nesprin3 to regulate cell migration in lung carcinoma. Oncology Reports. 2018; 40: 783–792. https://doi.org/10.3892/or.2018.6473.

[14] Knaup KX, Monti J, Hackenbeck T, Jobst-Schwan T, Klanke B, Schietke RE, *et al*. Hypoxia regulates the sperm associated antigen 4 (SPAG4) via HIF, which is expressed in renal clear cell carcinoma and promotes migration and invasion in vitro. Molecular Carcinogenesis. 2014; 53: 970–978. https://doi.org/10.1002/mc.22065.

[15] Liu T, Yu J, Ge C, Zhao F, Chen J, Miao C, *et al*. Sperm associated antigen 4 promotes SREBP1-mediated de novo lipogenesis via interaction with lamin A/C and contributes to tumor progression in hepatocellular carcinoma. Cancer Letters. 2022; 536: 215642. https://doi.org/10.1016/j.canlet.2022.215642.

[16] Wang Y, Tang Y, Li J, Wang D, Li W. Human sperm-associated antigen 4 as a potential prognostic biomarker of lung squamous cell carcinoma. The Journal of International Medical Research. 2021; 49: 3000605211032807. https://doi.org/10.1177/03000605211032807.

[17] Jayaraman S, Pazhani J, PriyaVeeraraghavan V, Raj AT, Somasundaram DB, Patil S. PCNA and Ki67: Prognostic proliferation markers for oral cancer. Oral Oncology. 2022; 130: 105943. https://doi.org/10.1016/j.oraloncology.2022.105943.

[18] Zhao J, Liu B, Yang JA, Tang D, Wang X, Chen Q. Human sperm-associated antigen 4 as a potential biomarker of glioblastoma progression and prognosis. Neuroreport. 2019; 30: 446–451. https://doi.org/10.1097/WNR.0000000000001226.

[19] Fatma H, Maurya SK, Siddique HR. Epigenetic modifications of c-MYC: Role in cancer cell reprogramming, progression and chemoresistance. Seminars in Cancer Biology. 2022; 83: 166–176. https://doi.org/10.1016/j.semcancer.2020.11.008.

[20] Wu G, Su J, Zeng L, Deng S, Huang X, Ye Y, *et al*. LncRNA BCAN-AS1 stabilizes c-Myc via N^6-methyladenosine-mediated binding with SNIP1 to promote pancreatic cancer. Cell Death and Differentiation. 2023; 30: 2213–2230. https://doi.org/10.1038/s41418-023-01225-x.

[21] Gao FY, Li XT, Xu K, Wang RT, Guan XX. c-MYC mediates the crosstalk between breast cancer cells and tumor microenvironment. Cell Communication and Signaling: CCS. 2023; 21: 28. https://doi.org/10.1186/s12964-023-01043-1.

[22] Meškytė EM, Keskas S, Ciribilli Y. MYC as a Multifaceted Regulator of Tumor Microenvironment Leading to Metastasis. International Journal of Molecular Sciences. 2020; 21: 7710. https://doi.org/10.3390/ijms21207710.

[23] Lin J, Wang X, Zhai S, Shi M, Peng C, Deng X, *et al*. Hypoxia-induced exosomal circPDK1 promotes pancreatic cancer glycolysis via c-myc activation by modulating miR-628-3p/BPTF axis and degrading BIN1. Journal of Hematology & Oncology. 2022; 15: 128. https://doi.org/10.1186/s13045-022-01348-7.

[24] Hu J, Duan W, Liu Y. Ketamine inhibits aerobic glycolysis in colorectal cancer cells by blocking the NMDA receptor-CaMK II-c-Myc pathway. Clinical and Experimental Pharmacology & Physiology. 2020; 47: 848–856. https://doi.org/10.1111/1440-1681.13248.

[25] He T, Zhou H, Li C, Chen Y, Chen X, Li C, *et al*. Methylglyoxal suppresses human colon cancer cell lines and tumor growth in a mouse model by impairing glycolytic metabolism of cancer cells associated with down-regulation of c-Myc expression. Cancer Biology & Therapy. 2016; 17: 955–965. https://doi.org/10.1080/15384047.2016.1210736.

[26] Xu D, Ma R, Ju Y, Song X, Niu B, Hong W, *et al*. Cholesterol sulfate alleviates ulcerative colitis by promoting cholesterol biosynthesis in colonic epithelial cells. Nature Communications. 2022; 13: 4428. https://doi.org/10.1038/s41467-022-32158-7.